Scaling theory for steady-state plastic flows in amorphous solids

Edan Lerner and Itamar Procaccia
Department of Chemical Physics, The Weizmann Institute of Science, Rehovot 76100, Israel
(Received 20 May 2009; published 26 August 2009)

Strongly correlated amorphous solids are a class of glass formers whose interparticle potential admits an approximate inverse power-law form in a relevant range of interparticle distances. We study the steady-state plastic flow of such systems, first in the athermal quasistatic limit and second at finite temperatures and strain rates. In all cases we demonstrate the usefulness of scaling concepts to reduce the data to universal scaling functions where the scaling exponents are determined *a priori* from the interparticle potential. In particular we show that the steady plastic flow at finite temperatures with efficient heat extraction is uniquely characterized by two scaled variables; equivalently, the steady-state displays an equation of state that relates one scaled variable to the other two. We discuss the range of applicability of the scaling theory, and the connection to density scaling in supercooled liquid dynamics. We explain that the description of transient states calls for additional state variables whose identity is still far from obvious.

DOI: 10.1103/PhysRevE.80.026128 PACS number(s): 62.20.fq, 61.43.Fs

I. INTRODUCTION

The equations of fluid mechanics appear to provide an adequate description for the flow of liquids for an extremely wide range of boundary conditions and external forcing. A similarly successful theory is still lacking for the description of elastoplastic dynamics in amorphous solids which form as the result of the glass transition. While being essentially "frozen liquids," amorphous solids differ from regular liquids in having a yield strength σ_s, a material parameter which depends on the density, temperature, etc, which is the maximal value of the internal stress that the material can support by elastic forces. Regular liquids cannot support any amount of stress without flowing. When the stress exceeds the yield strength the material begins to respond plastically, and under a given external shear rate can develop a steady-state plastic flow with a mean "flow stress" σ_∞. The analog of the Navier-Stokes equations which can describe the whole spectrum of elastoplastic responses in terms of macroscopic variables is not known yet, and their derivation is the subject of much current research [1–9] with significant amount of debate. In this paper we focus attention on the steady-state plastic flow which is obtained under the action of a constant external strain rate. We will argue below that the characterization of such a state is considerably simpler than the full description of transient states, the latter call for a larger number of macroscopic variables whose nature is not obvious and the constitutive relations between them are not known. For the steady plastic flow state we can make progress and determine what are the state variables that determine the state uniquely.

To simplify things further we limit our attention at present to materials whose interparticle potential can be approximated, for the range of interparticle distances of relevance, by an inverse power-law potential. This same class of materials and the interesting scaling properties that they exhibit attracted considerable interest in the context of the dynamics of supercooled liquids, first experimentally [13–16] and then theoretically [17–20]. In the context of the mechanical properties of amorphous solids we believe that the first example of using the special scaling properties of these materials appeared in [3] where focus was put on the athermal limit and quasistatic strain. In this paper we explore further the quasistatic limit, and then extend the discussion to systems at finite temperatures and finite strain rates. The discussion culminates with finding which are the minimal number of rescaled state variables that determine uniquely the steady plastic flow in such materials. Any general theory that attempts to provide a complete description of elastoplasticity in amorphous solids should reduce, in the steady flow state of materials of the present class, to a theory that contains these and only these variables.

The structure of the paper is as follows: in Sec. II we introduce the systems under study, and explain how they are simulated both in the athermal quasistatic limit and at finite temperatures and strain rates. In Sec. III we explain the special scaling properties that these systems possess, and predict theoretically what is expected in the steady plastic flow state. This is the central part of the paper. We then provide detailed presentations of simulation results and demonstrate how they compare to the predictions of the scaling theory. We discuss analytic properties of the scaling function, and demonstrate the conditions under which the scaling breaks down. In Sec. IV we discuss the consequences of our thinking to supercooled liquids, and propose that the scaling function used in the literature in this context are incomplete. Sec. V summarizes the findings, and provides a discussion of the road ahead, especially in terms of extensions to transient states.

II. SYSTEMS AND METHODS OF SIMULATION

A. System Definitions

In this work we employ two-dimensional polydisperse systems of point particles of equal mass m, interacting via two qualitatively different pairwise potentials. Each particle i is assigned an interaction parameter λ_i from a normal distribution with mean $\langle\lambda_i\rangle=1$. The variance is governed by the polydispersity parameter $\Delta=15\%$ where $\Delta^2=\frac{\langle(\lambda_i-\langle\lambda\rangle)^2\rangle}{\langle\lambda\rangle^2}$. With the definition $\lambda_{ij}=\frac{1}{2}(\lambda_i+\lambda_j)$ the first potential $U_R(r_{ij})$ is purely repulsive, of which the shape is characterized by theinterger k:

$$U_R(r_{ij}) = \begin{cases} \epsilon\left[\left(\frac{\lambda_{ij}}{r_{ij}}\right)^k - \frac{k(k+2)}{8}\left(\frac{B_0}{k}\right)^{(k+4)/(k+2)}\left(\frac{r_{ij}}{\lambda_{ij}}\right)^4 + \frac{B_0(k+4)}{4}\left(\frac{r_{ij}}{\lambda_{ij}}\right)^2 - \frac{(k+2)(k+4)}{8}\left(\frac{B_0}{k}\right)^{k/(k+2)}\right], & r_{ij} \le \lambda_{ij}\left(\frac{k}{B_0}\right)^{1/(k+2)} \\ 0, & r_{ij} > \lambda_{ij}\left(\frac{k}{B_0}\right)^{1/(k+2)} \end{cases}, \tag{1}$$

We chose $B_0=0.2$ for all systems discussed, and vary the integer k in the following. This pairwise potential is constructed such as to minimize computation time, and is smooth up to second derivative, which is required for minimization procedures.

The second pairwise potential $U_A(r_{ij})$ reads

$$U_A(r_{ij}) = \begin{cases} \tilde{U}(r_{ij}), & r \le r_\star(\lambda_{ij}) \\ \hat{U}(r_{ij}), & r_\star(\lambda_{ij}) < r \le r_c(\lambda_{ij}) \\ 0, & r > r_c(\lambda_{ij}) \end{cases} \tag{2}$$

with $\tilde{U}(r_{ij})=\epsilon[(\frac{\lambda_{ij}}{r_{ij}})^k-(\frac{\lambda_{ij}}{r_{ij}})^6-1/4]$; $k=12$, $r_\star=2^{1/6}\lambda_{ij}$, and $r_c=1.36\lambda_{ij}$. The attractive part $\hat{U}(r)$ is glued smoothly to the repulsive part. We choose $\hat{U}(r)=\frac{\epsilon}{2}P(\frac{r-r_0}{r_c-r_0})$ where $P(x)=\Sigma_{i=0}^5 A_i x^i$ and the coefficients A_i (see Table I) are chosen such that the potential is smooth up to second derivative. These pairwise potentials are displayed in Fig. 1 for the cases of interest. Below the units of length, energy, mass, and temperature are $\lambda \equiv \langle \lambda_i \rangle$, ϵ, m, and ϵ/k_B where k_B is Boltzmann's constant. The time units $\tau_\star$ are accordingly $\tau_\star=\sqrt{m\lambda^2/\epsilon}$. From here and in the following we denote the density as $\tilde{\rho} \equiv \frac{N}{V}$, and define the dimensionless density $\rho \equiv \lambda^d \tilde{\rho}$. Also, we will refer to the dimensionless density as just the density, for the sake of brevity.

Initial conditions for all the simulations, for both methods described in the next subsection, were obtained by instantaneous quenching of random, high-temperature configurations; this explains the apparent noise and absence of stress peaks in the transients. Furthermore, it is important to note that due to finite system sizes, the initial value of the stress of the quenched configurations in some experiments is nonzero; this is however irrelevant for steady-state statistics.

B. Methods

The work presented here is based on two types of simulational methods. The first type corresponds to the athermal quasistatic (AQS) limit $T \to 0$ and $\dot{\gamma} \to 0$, where $\dot{\gamma}$ is the strain rate. AQS methods have been extensively used recently [4–9] as a tool for investigating plasticity in amorphous systems. The order in which the limits $T \to 0$, $\dot{\gamma} \to 0$ are taken is important, since one expects that at any finite temperature the stress in the system can thermally relax given long enough time [10] (or small enough strain rates), hence the limit $T \to 0$ should be taken prior to the $\dot{\gamma} \to 0$ limit. According to AQS methods, starting from a completely quenched configuration of the system, we apply an affine simple shear transformation to each particle i in our shear cell, according to

$$r_{ix} \to r_{ix} + r_{iy}\delta\epsilon, \qquad r_{iy} \to r_{iy}, \tag{3}$$

in addition to imposing Lees-Edwards boundary conditions [11]. The strain increment $\delta\epsilon$ plays a role analogous to the integration step in standard molecular dynamics (MD) simulations. We choose for the discussed systems $\delta\epsilon=10^{-4}$, which while not sufficiently small for extracting exact statistics of plastic flow events as done in [8], it is, however, sufficiently small for the analysis of the steady-state properties and mean values. The affine transformation Eq. (3) is then followed by the minimization [12] of the potential energy under the constraints imposed by the strain increment and the periodic boundary conditions. We chose the termination threshold of the minimizations to be $|\nabla U|^2/N^2=10^{-18}$.

TABLE I. The coefficients in $P(x)=\Sigma_{i=0}^5 A_i x^i$, see text.

A_0	−1.0
A_1	0.0
A_2	0.806111631332424
A_3	7.581665106002721
A_4	−12.581665106002717
A_5	5.193888368667571

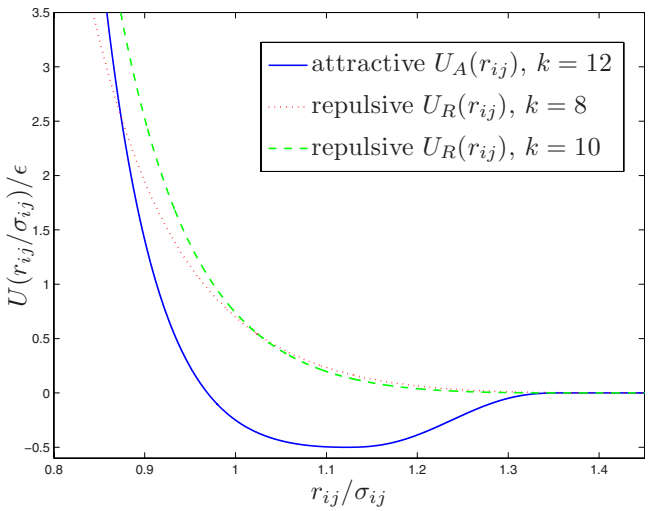

FIG. 1. (Color online) The different pairwise potentials discussed in this work.

The second simulation method employs the so-called Sllod equations of motion [11]. For our constant strain rate two-dimensional systems, they read

$$\dot{r}_{ix} = p_{ix}/m + \dot{\gamma} r_{iy},$$

$$\dot{r}_{iy} = p_{iy}/m,$$

$$\dot{p}_{ix} = f_{ix} - \dot{\gamma} p_{iy},$$

$$\dot{p}_{iy} = f_{iy}.$$

We use a leapfrog integration scheme for the above equations, and keep the temperature constant by employing the Berendsen thermostat [11], measuring the instantaneous temperature with respect to a homogeneous shear flow. The integration time steps were varied between $\delta t = 0.007$ and $\delta t = 0.001$, depending on density, such that numerical stability was maintained for all densities simulated. The time scale τ_T for heat extraction [11] was chosen such that rate of heat generation is smaller than the rate of heat extraction. For the lowest densities this was chosen to be $\tau_T \approx 10\tau_\star$.

III. SCALING THEORY

The discussion of the relaxation properties of glass formers in the supercooled regime [13–20] and of the mechanical properties of the amorphous solids [3] simplifies significantly when the interparticle potential assumes an effective inverse power law from in the relevant range of interparticle distances. As an example consider the potential Eq. (1) in the density range $\rho \in [1, 1.6]$. Since in d dimensions the characteristic interparticle distance r_0 scales such as

$$r_0 \sim \frac{\lambda}{\rho^{1/d}}, \tag{4}$$

the range of densities employed here is equivalent to a range of $r_0/\lambda \in [\rho_{\max}^{-1/d}, \rho_{\min}^{-1/d}]$. We find that in this range, to a very good approximation,

$$\frac{1}{r^{d-1}} \frac{\partial U_R(r)}{\partial r} \sim \frac{\epsilon}{\lambda^d} \left(\frac{r}{\lambda} \right)^{-\nu d}. \tag{5}$$

In two dimensions $\nu = 4.80$ for $k=8$ and $\nu = 5.87$ for $k=10$, see Fig. 2.

In the following discussion we define the flow stress σ_∞ to be the steady-state value of the stress under constant external strain rate. In general, the flow stress is a function of a set of state variables, which specify the conditions in which the experiments are carried out. For the systems and experiments discussed in this work, the flow stress depends on the density ρ, the temperature T, and the strain rate $\dot{\gamma}$. In addition, one can expect also a dependence on the heat extraction rate τ_T^{-1}. We choose to exclude the latter from the present discussion, and we do so by choosing the rate of heat extraction to be much larger than the rate of heat production. So, we propose at this point that $\sigma_\infty = \sigma_\infty(T, \rho, \dot{\gamma})$. The yield stress $\sigma_Y(\rho)$ is defined as the steady-state value of the stress under the limits $T \to 0$ and $\dot{\gamma} \to 0$ (see discussion regarding these limits in Sec. III C), i.e.,

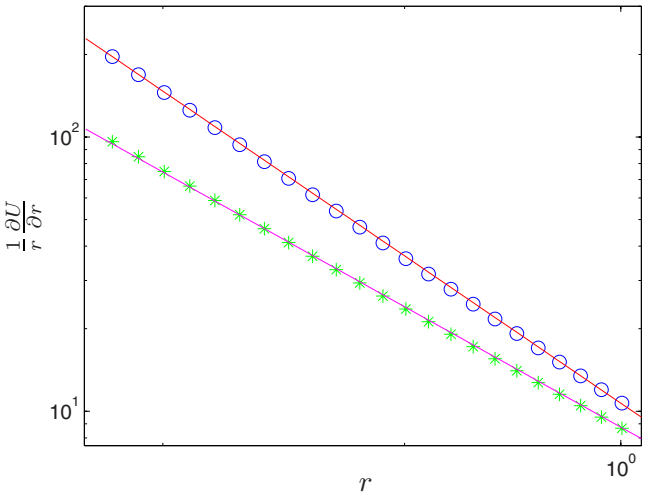

FIG. 2. (Color online) $r^{-1}\frac{\partial U(r)}{\partial r}$ in the range of $r_0/\lambda \in [\rho_{\max}^{-1/2}, \rho_{\min}^{-1/2}]$ for $k=8$ in green asterisks, and for $k=10$ in blue circles. The line through the points represents the scaling laws Eq. (5)

$$\sigma_Y \equiv \sigma_\infty(\rho, T \to 0, \dot{\gamma} \to 0). \tag{6}$$

A. Scaling in the athermal quasistatic limit

In the athermal quasistatic limit the only parameter left is the density; consideration of the temperature and strain rate effects will be taken up in the next subsection. Denote the distribution of interparticle distances as $p(r)$; then the mean interparticle distance is $r_0(\rho) \equiv \int r p(r;\rho) dr$. Note that this probability distribution only accounts for distances which are relevant in terms of the interaction, namely, for $r_{ij} \le \lambda_{ij} (\frac{k}{B_0})^{1/(k+2)}$. If $p(r)$ is sufficiently sharply peaked around r_0, we can write

$$\left\langle r \frac{\partial U_R}{\partial r} \right\rangle \sim r_0 \left. \frac{\partial U_R}{\partial r} \right|_{r_0} \sim \epsilon \left(\frac{r_0}{\lambda} \right)^{d(1-\nu)} \sim \epsilon \rho^{\nu - 1}. \tag{7}$$

From here we predict that for our systems with short-range forces the scaling of the yield stress should be

$$\sigma_Y \sim N \frac{r_0 \left. \frac{\partial U_R}{\partial r} \right|_{r_0}}{V} \sim \frac{\epsilon}{\lambda^d} \rho^\nu. \tag{8}$$

In the athermal quasistatic limit the shear modulus μ, which is measured as the average of $\partial\sigma/\partial\gamma$ over the elastic branches, must obey the same scaling

$$\mu \sim \frac{\epsilon}{\lambda^d} \rho^\nu. \tag{9}$$

These scaling laws lead to the expectation that replotting stress-strain curves in terms of rescaled variable σ/ρ^ν should result in complete data collapse. Indeed, our simulations vindicate this expectation. In Fig. 3 we present the raw stress-strain curves in the athermal quasistatic limit using seven different values of the density. For each density we simulated 20 independent runs of $N=4096$ particles, using the pairwise

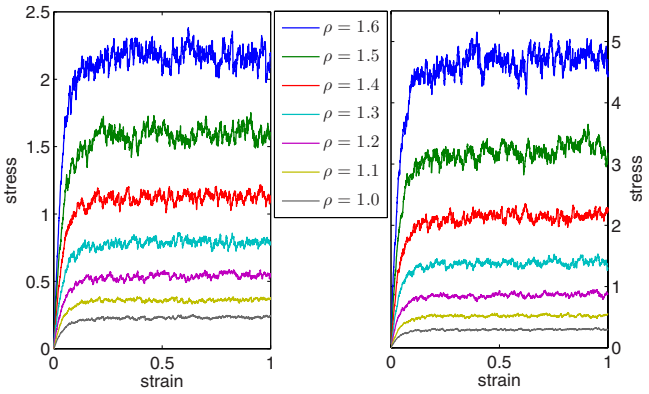

FIG. 3. (Color online) Stress-strain curves averaged over 20 independent runs for an athermal system with $N=4096$, $k=8$ (left panel) and $k=10$ (right panel) as a function of the density, with the density increasing from bottom to top.

potential Eq. (1) and two choices of the integers $k=8$ and $k=10$. Figure 4 demonstrates the superb data collapse for the scaled variable. The insets are a direct test of the scaling laws Eqs. (8) and (9).

B. Scaling theory with temperature and external strain rate

Once we perform measurements at finite temperatures and external strain rates the scaling considerations must incorporate temporal and energy scales. The typical elastic energy density in the steady-state plastic flow should scale like σ_Y^2/μ. Accordingly, the intensive energetic contribution to barriers δG (that govern thermal activation) scales with the density according to

$$\langle \delta G \rangle \sim \frac{V\frac{\sigma_Y^2}{\mu}}{N} \sim \epsilon \rho^{\nu-1}. \tag{10}$$

Note that this is the "density scaling" proposed in [13–20] in the context of the dynamics of supercooled liquids. For the present purposes we need to explore further scaling relations; we estimate now the density scaling of the typical time scale τ_0 with respect to which all the rates in the theory should be compared. We begin with the speed of sound c_s; using Eq. (9) we write

$$c_s = \sqrt{\frac{\mu}{\rho}} \sim \frac{\lambda}{\tau_\star}\rho^{(\nu-1)/2}. \tag{11}$$

We can now define the time scale $\tau_0 \equiv r_0/c_s$; using Eqs. (4) and (11) we obtain

$$\tau_0 \sim \tau_\star \rho^{-(\nu d-d+2)/(2d)}. \tag{12}$$

Using Eq. (10) we conclude that the effect of temperature on the dynamics in the steady-state must be invariant once the temperature is rescaled by $\rho^{\nu-1}$. On the other hand the external strain rate $\dot{\gamma}$ should leave the system invariant once rescaled by $\rho^{-(\nu d-d+2)/(2d)}$ due to Eq. (12). Putting together all these we finally propose the expected scaling function form for the flow stress σ_∞:

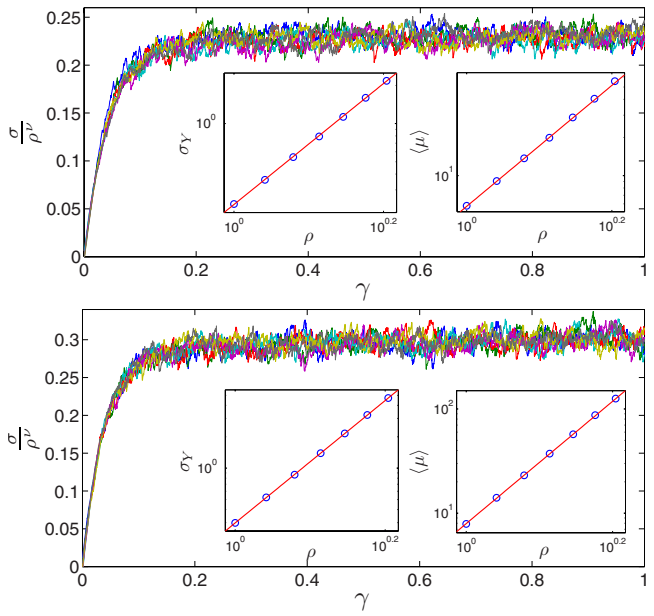

FIG. 4. (Color online) The same stress-strain curves as in Fig. 3 but with the stress rescaled by ρ^ν, with $\nu=4.80$ for $k=8$ (top panel) and $\nu=5.87$ for $k=10$ (bottom panel). The insets demonstrate the density dependence of σ_Y and μ according to ρ^ν.

$$\sigma_\infty(T,\rho,\dot{\gamma}) = \frac{\epsilon}{\lambda^d}\rho^\nu \mathcal{S}\left(\frac{T}{\epsilon\rho^{\nu-1}}, \frac{\dot{\gamma}}{\tau_\star^{-1}\rho^{(\nu d-d+2)/(2d)}}\right). \tag{13}$$

This is the central theoretical result of this section. We stress that we chose to favor the flow stress and wrote it in terms of the scaling function of the other two dimensionless variables. We could equivalently choose any of the other two variables to be represented in an analog way in terms of two dimensionless variables. This scaling function form is in fact an equation of state for the steady plastic flow.

For $d=2$ this general result assumes the form

$$\sigma_\infty(T,\rho,\dot{\gamma}) = \frac{\epsilon}{\lambda^2}\rho^\nu \mathcal{S}\left(\frac{T}{\epsilon\rho^{\nu-1}}, \frac{\dot{\gamma}}{\tau_\star^{-1}\rho^{\nu/2}}\right). \tag{14}$$

To demonstrate the high degree of precision with which the scaling theory is obeyed we performed simulations at finite temperature and strain rate (see methods section) in which we prepared 10 independent systems (for each density) of $N=10000$ particles at the densities $\rho=1.0$, 1.1, 1.2, 1.3, and 1.4. Defining the two dimensionless variable $x \equiv \frac{T}{\epsilon\rho^{\nu-1}}$ and $y \equiv \frac{\dot{\gamma}}{\tau_\star^{-1}\rho^{\nu/2}}$, we fix the value $y_0=1.6\times10^{-5}$ for all densities, and simulated all the five densities for the values $x=0.001$, 0.01, 0.1, and 0.2. The results are displayed in Fig. 5. We see the excellent data collapse and also the quality of the scaling laws for the flow stress; the slopes of the lines in the right panels are those predicted theoretically in Eq. (13), i.e., $\sigma_\infty \sim \frac{\epsilon}{\lambda^2}\rho^\nu$.

We now test the quality of the prediction of the existence of the scaling function $\mathcal{S}(x,y)$. To this aim we fixed a value of $\rho=1.15$ and the same $y_0=1.6\times10^{-5}$, and simulated the entire range of x values for which $\mathcal{S}(x,y)$ exists. The result is shown in Fig. 6, in addition to the data obtained for all the

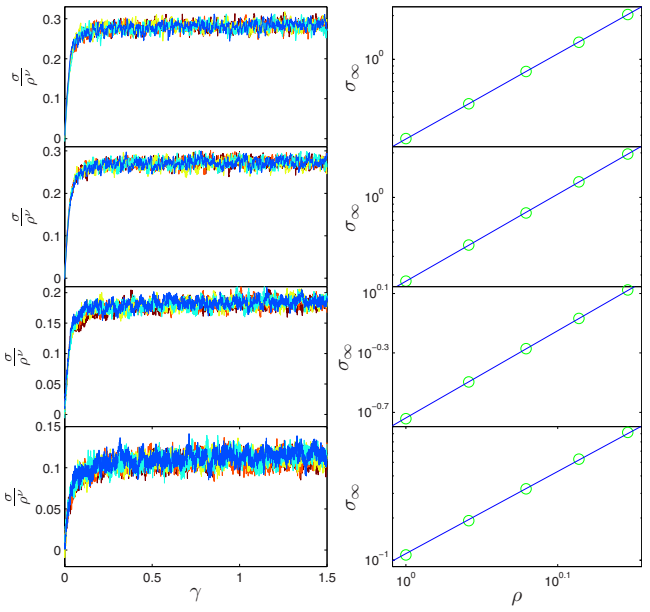

FIG. 5. (Color online) Left panels: stress normalized by ρ^ν vs strain for the x values $x=0.001$, $x=0.01$, $x=0.1$, and $x=0.2$, increasing from top to bottom. Right panels: log-log plots of the steady-state flow stress as a function of density, for the same corresponding values of x.

other densities and x values shown in Fig. 5. The excellent data collapse is quite apparent. It is noteworthy that at low temperatures the function reaches smoothly, albeit with a very high gradient, precisely the athermal quasistatic limit that was studied in the previous subsection. The high gradient as $T\to 0$ in a similar, experimentally obtained function, was interpreted in [21] as resulting from quantum-mechanical effects. Obviously in our purely classical simulations there are no quantum effects and it remains very interesting to unfathom the origin of the very fast change in the

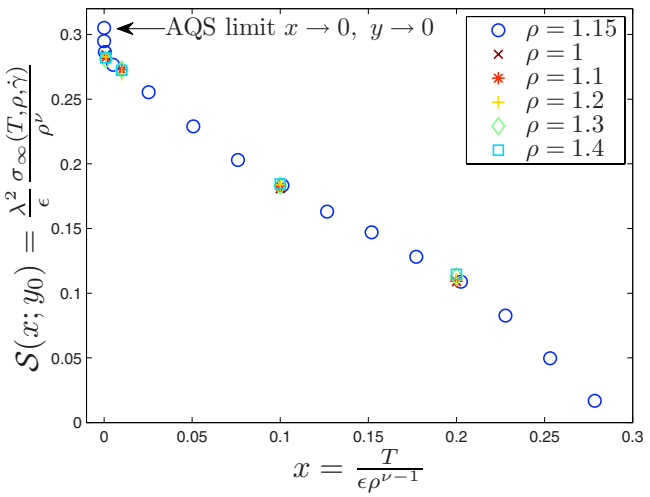

FIG. 6. (Color online) The function $\mathcal{S}(x;y_0)$. Data is displayed for $\rho=1.15$ (blue circles) over a wide range of $x=\frac{T}{\epsilon\rho^{\nu-1}}$ values, and for the densities of Fig. 5 over the x values $x=0.001$, $x=0.01$, $x=0.1$, and $x=0.2$. The value of $y_0=\frac{\dot\gamma}{\tau_\star^{-1}\rho^{\nu/2}}$ is 1.658×10^{-5} for all simulated systems.

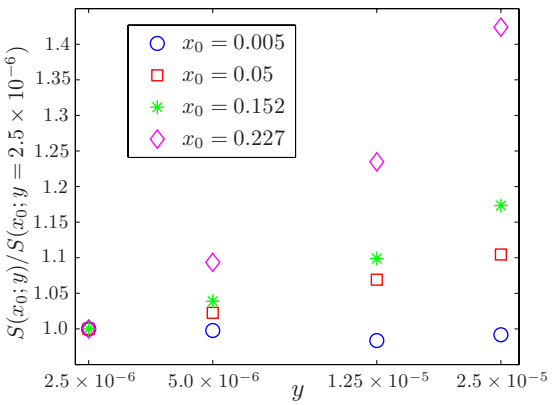

FIG. 7. (Color online) The scaling function $\mathcal{S}(x_0,y)$ normalized by the values $\mathcal{S}(x_0,y=2.5\times 10^{-6})$, for various values of y.

flow stress over a very short temperature interval.

To emphasize the relevance of the temporal scaling we simulated steady flow states at different external strain rates but at the same x values. The result are shown in Fig. 7. We see that as the temperature increases, the relative sensitivity of the flow stress to changes in the the strain rate increases appreciably. Note that the value of $y_0=1.6\times 10^{-5}$ for which the data collapse was demonstrated is well within the range of high sensitivity to changes in the strain rate. In other words, without rescaling the strain rate properly there is no hope for data collapse. Further analytic properties of the scaling function are discussed in the next subsection.

C. Analytic properties of the scaling function

The entire physics of the steady flow state for this class of systems is encoded in the scaling function $\mathcal{S}(x,y)$. It is therefore very challenging to derive the form of this functions from first principles. We are not yet in a position to do so; at this point we can only present the analytic properties of this function as a preparation for future discussions.

First, it is noteworthy that the limits $\lim_{x\to 0}\lim_{y\to 0}$ and $\lim_{y\to 0}\lim_{x\to 0}$ do not commute. We expect that

$$\lim_{x\to 0}\lim_{y\to 0}\mathcal{S}(x,y)=0, \tag{15}$$

simply because at any finite temperature, given enough time to relax the stress, the flow stress must vanish [10]. On the other hand

$$\lim_{y\to 0}\lim_{x\to 0}\mathcal{S}(x,y)=\sigma_Y/\rho^\nu, \tag{16}$$

as can be seen directly from Fig. 6.

Second, in the athermal limit $x\to 0$ the flow stress loses its dependence on the external strain rate for sufficiently small values of y,

$$\lim_{y\to 0}\lim_{x\to 0}\frac{\partial\mathcal{S}(x,y)}{\partial y}=0. \tag{17}$$

This property can be seen directly in Fig. 7. The physical reason for this property is that without substantial thermal activation the physics becomes insensitive to external time

scales. This limit is expected to hold when the external strain rate is much smaller than the elastic relaxation rate; interplays between high strain rates and the flow stress were investigated in [22].

Finally, we observe an inflection point in $\mathcal{S}(x,y)$, see Fig. 6 around $x=0.1$, where

$$\left.\frac{\partial^2 \mathcal{S}(x,y)}{\partial x^2}\right|_y = 0. \tag{18}$$

We conjecture that this inflection point separates a "low-temperature region" from a "high-temperature region" in which the elastoplastic physics is not the same. It is possible that a change from delocalized plastic events to more localized events [8,22] is the fundamental reason for this change, but further study is necessary to pinpoint this issue in a convincing way.

D. Applicability of the scaling theory

At this point it is appropriate to discuss the general applicability of the scaling approach. It is sufficient to delineate this applicability in the context of the athermal, quasistatic limit using systems in which the interparticle potential cannot be usefully approximated as inverse power laws. In some model systems, e.g [19], it has been shown that density scaling of the dynamics of supercooled liquids still holds in spite of the presence of attractive forces in the potential. Furthermore, the same qualitative density scaling has been applied to a wide variety of experimental data, with substantial success [13–16]. In these experimental systems there are definitely attractive forces between the particles, and thus the question of the applicability of the scaling theory is highly pertinent.

1. Simulations

We have simulated systems with the potential $U_A(r)$, Eq. (2) in the athermal quasistatic limit. In this potential an attractive branch is added to the repulsive one, see Fig. 1. We again prepared 20 independent runs for each of the seven densities $\rho=1.0$, 1.1, 1.2, 1.3, 1.4, 1.5, and 1.6, this time for systems of $N=2500$ particles, and collected statistics for the steady-state stress values (see methods section), as previously described.

The raw data of the stress-strain curves is displayed in the left panel of Fig. 8. In the right upper panel we show what happens when we try to collapse the data by rescaling the stress by σ_Y. Of course the stress-stain curves now all asymptote to the same value, but the curves fail to collapse, since $\langle\mu\rangle$ does not scale in the same way as σ_Y. Nevertheless, even in the present case we can have predictive power for high densities. When the density increases the repulsive part of the potential Eq. (2) becomes increasingly more relevant, and the inner power-law r^{-12} becomes dominant. We therefore expect that for higher densities scaling will be regained, and both σ_Y and $\langle\mu\rangle$ would depend on the density as ρ^7. The two lower right panels in Fig. 8 show how well this prediction is realized also in the present case.

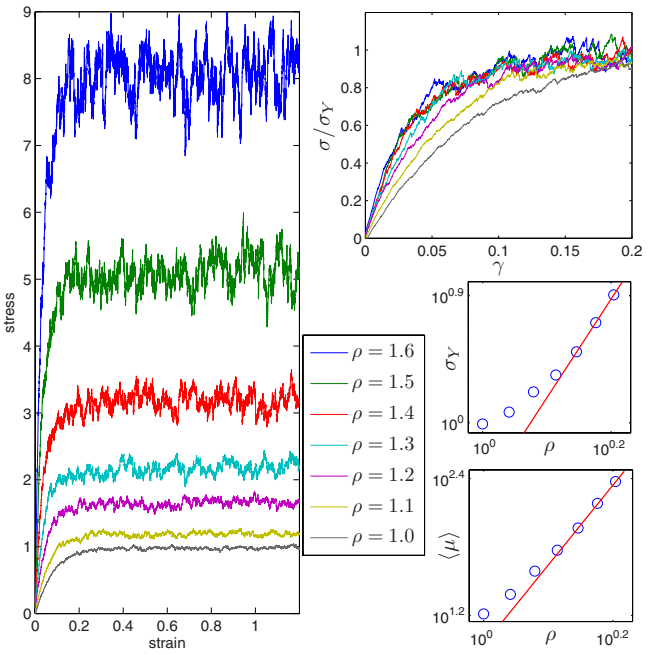

FIG. 8. (Color online) Left panel: stress-strain curves for the potential Eq. (2) which has a repulsive and an attractive part for all densities increasing from bottom to top. Right upper panel: demonstration of the failure of rescaling of the stress-strain curves. Lower panels: σ_Y and $\langle\mu\rangle$ as a function of the density. Note that predictability is regained only for higher densities, the straight line is ρ^7.

2. Constancy of the ratio of the shear modulus and the yield stress

Another way of flushing out the failure of scaling when there exist attractive forces is provided by the ratio

$$\Omega \equiv \frac{\mu}{\sigma_Y}. \tag{19}$$

This is a pure number, which has been claimed to be universal for a family of metallic glasses [21]. For systems in which our scaling analysis holds, we have seen that the shear modulus scales with density in exactly the same manner as the yield stress [see Eqs. (8) and (9)], hence the number Ω should be invariant to density changes, for a given system. However, when compared across different systems, there is no *a priori* reason to expect this number to be universal. Figure 9 displays the measured values of Ω for our athermal quasistatic experiments, for two different repulsive potentials of the form (1), using $k=8$ and $k=10$, and for the attractive potential Eq. (2), with $k=12$. For the two repulsive potentials, we find from our numerics that this parameter differs by about 5%, indicating nonuniversality. The lack of universality is even clearer with the last potential Eq. (2). It is apparent that when scaling prevails the value of Ω is constant up to numerical fluctuations. In the third case, where scaling fails, Ω is a strong function of ρ except at higher densities where scaling behavior is recaptured as explained. We can therefore conclude that the approximate constancy of Ω found in a family of metallic glasses [21], is not fundamental but only an indication of the similarity of the poten-

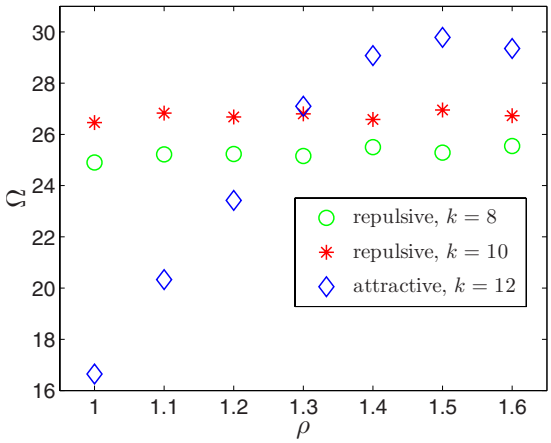

FIG. 9. (Color online) The pure number Ω as a function of the density for the three potentials discussed in the text. Note that Ω appears to increase with the exponent of the repulsive part of the potential whenever scaling prevails.

tials for this family. In general Ω can depend on the interparticle potential. It is quite clear from considering Eqs. (7)–(9), that the *coefficients* in the scaling laws Eqs. (8) and (9) may well depend on the exponent k in the repulsive part of the potential. The ratio of these prefactors, being a pure number, could be independent of k, and Ω could be universal. It appears however that $\langle \mu \rangle$ is increasing more with k than σ_Y, and therefore Ω shows a clear increase upon increasing k. At present this must remain an interesting riddle for future research.

IV. RELATION TO DENSITY SCALING IN SUPERCOOLED LIQUIDS

The destruction of scaling for low-density systems with the attractive potential Eq. (2) is in apparent contradiction to density scaling analysis of relaxation times in supercooled liquids. As mentioned above, it has been shown in the context of the dynamics of supercooled liquids, both in model systems and in experiments, that the presence of attractive forces in the pairwise potentials can still be consistent with density scaling. In our context of mechanical properties scaling is regained only at high densities; it is desirable to understand whether there is a qualitative difference between the influence of attractive forces on mechanical properties, and the influence of attractive forces on the dynamics of supercooled liquids.

The standard way in which density scaling is presented in the context of the dynamics of supercooled liquids is in the form [13–16,18,19]

$$\tau_\alpha(T,\rho) = \mathcal{F}\left(\frac{T}{\rho^\gamma}\right), \tag{20}$$

where τ_α is the α-relaxation time and $\mathcal{F}(x)$ is a scaling function of one rescaled variable; the exponent γ corresponds to $\nu-1$ in our scaling analysis.

In our opinion this form cannot be exact, and we propose now an alternative form in light of the analysis presented above. The form (20) account only for the density scaling of the free-energy barriers for thermal activation. We have noted above that on top of this the microscopic time scale τ_0, with respect to which rates are compared, also varies with density, see Eq. (12) and discussion in Sec. III B.

Write the α-relaxation time in the standard transition-state-theory form

$$\tau_\alpha(T,\rho) = \tau_0 e^{\delta G(T)/T}. \tag{21}$$

The free-energy barrier δG scales with density as $\delta G \sim \epsilon \rho^{\nu-1}$ [see discussion prior to Eq. (10)]; the microscopic time scale should scale as $\tau_0 \sim \tau_\star \rho^{-(\nu d-d+2)/(2d)}$, [see discussion prior to Eq. (12)]. Combining these considerations, we obtain the scaling form

$$\tau_\alpha(T,\rho) = \tau_\star \rho^{-(\nu d-d+2)/(2d)} \mathcal{F}\left(\frac{T}{\epsilon \rho^{\nu-1}}\right). \tag{22}$$

We believe that this correct form was missed because the scaling of thermal activation barriers appears in the exponent of the right-hand side of Eq. (21), whereas the scaling of the microscopic time scale is in the prefactor. Nevertheless it is our suggestion that data should be reanalyzed using the proper form of the scaling function.

V. SUMMARY AND THE ROAD AHEAD

In this paper we offered some modest inroads into providing a theory for elastoplastic dynamics. We must admit that a complete theory of elastoplastic response of amorphous solids is still out of reach, mainly because of some fundamental riddles that are highly debated. Our proposition in this paper is that understanding the steady plastic flow state is first simpler than and second mandatory for achieving a full theory of elastoplasticity. By focusing on glass formers with simple effective inverse power-law potentials we achieved a scaling theory for the steady-state flow stress under constant strain rate and finite temperatures. We have shown that in the athermal quasistatic limit the yield stress exhibits power-law dependence on the density, as does the shear modulus. It was then shown that temperature and external strain rate can be incorporated into the scaling approach by accounting for thermal activation effects via energy scaling, and rate effects via temporal scaling. The finite temperature and finite strain rate theory appears in excellent agreement with the athermal quasistatic limit when the appropriate limits are taken.

The first task ahead is to provide an understanding from first principles of the scaling function $\mathcal{S}(x,y)$. We have discussed some analytical properties of this scaling function, some of which offer fascinating riddles for future research. Probably the most intriguing of these is the inflection point in $\mathcal{S}(x,y)$, see Eq. (18), and the corresponding discussion. Understanding the origin of this inflection point may shed light on the possibility of constructing mean field theories of plasticity at least for steady-states, including the external parameter regimes for which they might be valid.

Probably the most important remaining issue is the identification of additional state variable that are necessary to describe transient states. It is well known that after straining in one direction and reaching a steady-state, a change in straining direction with an angle with respect to the original direction results in angle-dependent trajectories. This means that a tensorial order parameter is written into the material during the steady flow state, and this object does not appear in our analysis. It must appear however in the transient trajectories. The identification of this tensorial object will call for additional future work.

ACKNOWLEDGMENTS

We have benefitted from discussions with George Hentschel. This work has been supported in part by the Israel Science Foundation, the German Israeli Foundation, and the Minerva Foundation, Munich, Germany.

[1] M. L. Falk and J. S. Langer, Phys. Rev. E **57**, 7192 (1998).
[2] M. J. Demkowicz and A. S. Argon, Phys. Rev. B **72**, 245205 (2005).
[3] E. Lerner, I. Procaccia, E. S. C. Ching, and H. G. E. Hentschel, Phys. Rev. B. **79**, 180203 (2009).
[4] C. E. Maloney and A. Lemaître, Phys. Rev. Lett. **93**, 016001 (2004).
[5] A. Tanguy, F. Leonforte, and J.-L. Barrat, Eur. Phys. J. E **20**, 355 (2006).
[6] C. E. Maloney and A. Lemaître, Phys. Rev. E **74**, 016118 (2006).
[7] N. P. Bailey, J. Schiøtz, A. Lemaître, and K. W. Jacobsen, Phys. Rev. Lett. **98**, 095501 (2007).
[8] E. Lerner and I. Procaccia, Phys. Rev. E **79**, 066109 (2009).
[9] M. Tsamados, A. Tanguy, F. Léonforte, and J.-L. Barrat, Eur. Phys. J. E **26**, 283 (2008).
[10] J.-P. Eckmann and I. Procaccia, Phys. Rev. E **78**, 011503 (2008).
[11] M. P. Allen and D. J. Tildesley, *Computer Simulations of Liquids* (Oxford University Press, London, 1991).
[12] A variant of the conjugate gradient algorithm was used, for details see http://www.inference.phy.cam.ac.uk/mackay/c/macopt.html.
[13] R. Casalini and C. M. Roland, Phys. Rev. E **69**, 062501 (2004).
[14] C. Alba-Simionesco, A. Cailliaux, A. Alegria, and G. Tarjus, Europhys. Lett. **68**, 58 (2004).
[15] C. Dreyfus, A. Le Grand, J. Gapinski, W. Steffen, and A. Patkowski, Eur. Phys. J. B **42**, 309 (2004).
[16] R. Casalini and C. M. Roland, Phys. Rev. B **71**, 014210 (2005).
[17] V. Ilyin, I. Procaccia, I. Regev, and N. Schupper, Phys. Rev. E **77**, 061509 (2008).
[18] U. R. Pedersen, N. P. Bailey, T. B. Schrøder, and J. C. Dyre, Phys. Rev. Lett. **100**, 015701 (2008).
[19] D. Coslovich and C. M. Roland, J. Phys. Chem. B **112**, 1329 (2008).
[20] N. P. Bailey, U. R. Pedersen, N. Gnan, T. B. Schrøder, and J. C. Dyre, J. Chem. Phys. **129**, 184507 (2008); **129**, 184508 (2008).
[21] W. L. Johnson and K. Samwer, Phys. Rev. Lett. **95**, 195501 (2005).
[22] A. Lemaître and C. Caroli, e-print arXiv:0903.3196.